High Resolution Photoelectron Spectroscopy of Cryogenically-Cooled NO_3^-

Mark C. Babin,[†] Jessalyn A. DeVine,[†] Martin DeWitt,[†] John F. Stanton,[▽,*] Daniel M. Neumark [†,⊥,*]

[†] Department of Chemistry, University of California, Berkeley, CA 94720, USA.

[▽] Quantum Theory Project, Department of Chemistry and Physics, University of Florida, Gainesville, Florida 32611, USA.

[⊥] Chemical Sciences Division, Lawrence Berkeley National Laboratory, Berkeley, CA 94720, USA.

Corresponding Authors

* johnstanton@ufl.edu, dneumark@berkeley.edu

ABSTRACT

High-resolution anion photoelectron spectra of cryogenically cooled NO_3^- anions obtained using slow photoelectron velocity-map imaging are presented and provide new insight into the vibronic structure of the corresponding neutral radical. A combination of improved spectral resolution, measurement of energy-dependent intensity effects, temperature control, and comparison to theory allows for full assignment of the vibronic features observed in this spectrum. We obtain a refined electron affinity of 3.9289(14) eV for NO_3. Further, the appearance of Franck-Condon forbidden transitions from vibrationally cold anions to neutral states with excitation along the NO_3 ν_4 mode confirms that these features arise from vibronic coupling with the $\tilde{B}^2E'$ excited state of NO_3 and are not hot bands as has been suggested. Together, the suite of experimental and simulated results provides clear evidence that the ν_3 fundamental of NO_3 resides near 1050 cm^{-1}, addressing a long-standing controversy surrounding this vibrational assignment.

TOC GRAPHICS

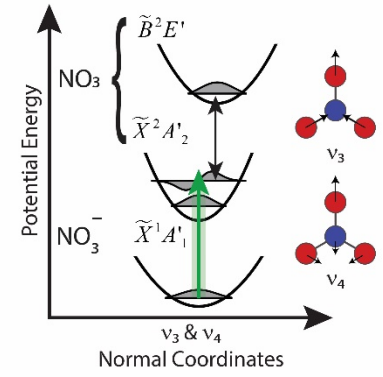

KEYWORDS photodetachment, vibronic coupling, spectroscopy, radicals

The nitrate radical (NO_3) was one of the first free radicals to be observed spectroscopically[1] and is one of the most important radicals in atmospheric chemistry. This species serves as the primary oxidizer in the nighttime troposphere, when photolysis by sunlight ceases and its concentration builds up.[2] Under these conditions, NO_3 reacts to form HNO_3, N_2O_5, and organic nitrates that are subsequently incorporated into aerosols, providing the largest source of uncertainty of the concentration of NO_x, O_3 and OH in atmospheric models.[3-5] This interesting chemistry has motivated numerous experiments utilizing FTIR,[6-15] dispersed fluorescence (DF),[16-18] diode laser spectroscopy,[19,20] matrix isolation spectroscopy,[21,22] cavity ringdown spectroscopy,[23,24] and anion photoelectron spectroscopy,[25] as well as several theoretical studies,[26-33] to characterize the electronic and vibrational structure of NO_3. Despite this extensive body of work, the nitrate radical still presents a significant challenge to both theory and experiment. In this Letter, we address questions recently posed in the literature about the vibronic structure of the $\widetilde{X}^2A'_2$ ground state of NO_3 using high resolution photoelectron spectroscopy of cryogenically cooled NO_3^- and accompanying theory.

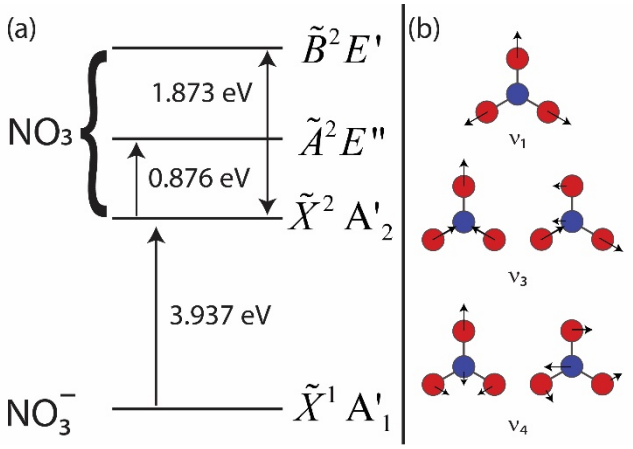

Figure 1. Electronic levels (a) and vibrational modes (b) in NO_3^- and NO_3.

The spectroscopy of NO_3 is complicated by the existence of two excited electronic states ($\widetilde{A}^2E''$ and $\widetilde{B}^2E'$) that lie roughly 1 and 2 eV, respectively, above the ground $\widetilde{X}^2A'_2$ state, as shown in Figure 1a. These three states exhibit a wealth of vibronic mixing that results from both Jahn-Teller (JT) and pseudo-Jahn-Teller (pJT) couplings.[24,25,27] The potential energy surface for the ground state is known to be quite flat by virtue of a strong $\widetilde{X}^2A'_2/\widetilde{B}^2E'$ pseudo-Jahn-Teller interaction, with both theory and experiment predicting symmetric (D_{3h}) and asymmetric (C_{2v}) structures at various times.[31-36] While the D_{3h} stationary point has not been unambiguously demonstrated to be a minimum or a (second-order) saddle point between equivalent C_{2v} structures, it is clear that the vibrationally averaged ground state structure has D_{3h} symmetry.[27]

Strong vibronic mixing between the ground $\widetilde{X}^2A'_2$ state with the $\widetilde{B}^2E'$ excited state was first suggested by Weaver *et al*,[25] whose photoelectron spectrum of NO_3^- is presented in Figure 2a. Peak **a**, located ~360 cm^{-1} above the 0_0^0 vibrational origin, was assigned to the Franck-Condon (FC) forbidden 4_0^1 transition involving the ν_4 degenerate bend of the neutral, which becomes allowed through pJT coupling. More recent theoretical work has shown that a relatively simple vibronic model accounts qualitatively for this behavior as well as a number of other spectroscopic properties of NO_3, such as the $\widetilde{X}-\widetilde{B}$ absorption spectrum and the DF spectrum in which the ground state is accessed from the lowest vibronic level of the $\widetilde{B}^2E'$ state.[27] This vibronic model also questioned the prior assignment of the strongest infrared absorption of NO_3 (~1492 cm^{-1}) to the ν_3 degenerate stretch,[20] ascribing it instead to a combination level; the true ν_3 position was calculated to be nearly 500 cm^{-1} lower. Subsequent and more quantitative work predicted that ν_3 and the totally symmetric stretch (ν_1) fundamentals reside close together (within 10 cm^{-1}), and that the former is the main contributor of intensity to the peak found ~1050 cm^{-1} above the origin, **b**, in

the NO_3^- photoelectron spectrum (Figure 2a). This implies that peak **b** may comprise both the FC-allowed 1_0^1 and FC-forbidden 3_0^1 transitions contradicting the original assignment to the 1_0^1 transition by Weaver *et al*.[26] The reassignment of the ν_3 frequency has led to a number of studies of the vibronic levels and spectra of NO_3.[6-8,10,11,14,21-23,37,38] Particularly noteworthy is a recent paper by Hirota[39] that questions the very existence of strong $\widetilde{X}^2A'_2/\widetilde{B}^2E'$ vibronic coupling, referencing work by Yamada and Ross[40] that claims peak **a** in Figure 2a was mis-assigned by Weaver *et al.* and instead corresponds to the FC-allowed 4_1^3 hot band.

The present study aims to address both of these critiques of the Weaver spectral assignments by using slow photoelectron velocity-map imaging of cryogenically-cooled anions (cryo-SEVI)[41] to revisit the photodetachment spectrum of NO_3^-. Compared to the experiments of Weaver *et al.*, cryo-SEVI offers considerably higher resolution, the removal of hot bands via cryogenic cooling of anions, and facile evaluation of the electron kinetic energy (eKE) dependence of peak intensities and photoelectron angular distributions (PADs). The latter two attributes shed light on the nature of the electronic states accessed by photodetachment, demonstrating that the ν_4 and ν_3 fundamentals in the $\widetilde{X}^2A'_2$ state of NO_3 gain intensity through vibronic coupling to the $\widetilde{B}^2E'$ state. We confirm the initial assignment set forth by Weaver for **a** as the ν_4 fundamental, and find that **b** is indeed dominated by the proximate 3_0^1 band. Excellent agreement between our

experimental spectra and high-level calculations affirms these assignments.

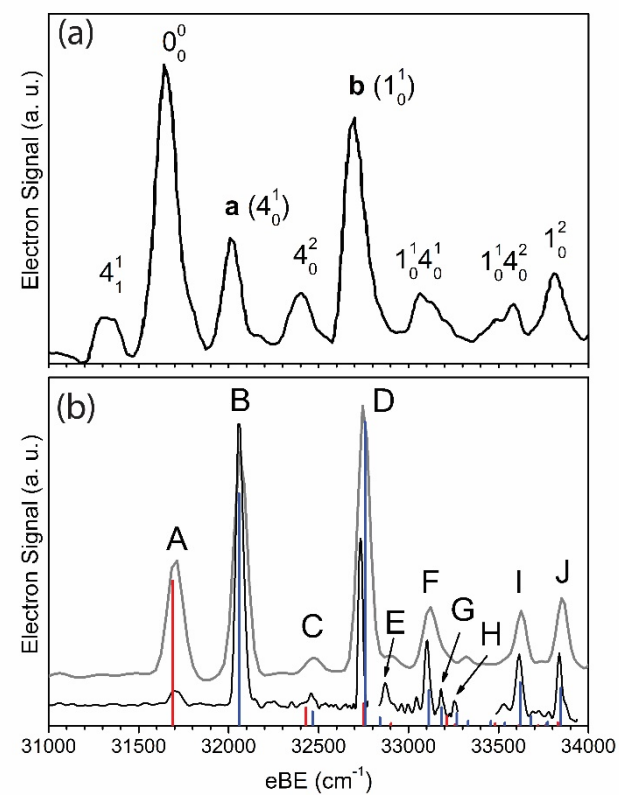

Figure 2. Photoelectron spectra of the of the $\widetilde{X}^2A'_2 \longleftarrow\!\!\!\!- \widetilde{X}^1A'_1$ transition of NO_3^- as reported in Ref 25 (a) and this work using cryo-SEVI (b). In (b), a low-resolution spectrum (grey, hν = 35137 cm^{-1}) sits above both high-resolution scans (black, variable photon energy) and a simulated photoelectron stick spectrum. Red sticks represent FC-allowed transitions and blue sticks represent transitions that gain intensity through pJT-coupling.

The cryo-SEVI spectrum of the $\widetilde{X}^2A'_2 \longleftarrow\!\!\!\!- \widetilde{X}^1A'_1$ photodetachment transition of NO_3^- is presented in Figure 2b, where a low-resolution overview spectrum is displayed atop high-resolution composite spectra taken at several photon energies. In addition, the cryo-SEVI results are compared to a simulated photoelectron stick spectrum, constructed using a 3-state Köppel-Domcke-Cederbaum (KDC) vibronic Hamiltonian for NO_3.[42] Electron binding energies (eBEs)

relative to the neutral electron affinity (EA) are given in Table 1 for all labelled transitions, alongside the KDC-predicted values and peak assignments. Details of the cryo-SEVI and theoretical methods are provided in Sections S1 and S2, respectively, of the Supporting Information (SI). A complete listing of the eigenvalues of the KDC Hamiltonian and the experimentally determined parameters with a comparison to literature values are presented in Tables S1 and S2, respectively, of the SI.

Table 1. Positions, shifts relative to the EA extracted from peak G (31689(11) cm^{-1}), assignments, and corresponding KDC eigenvalues for detachment transitions in the cryo-SEVI spectrum of NO_3^- presented in Figure 2b. Uncertainties in peak positions correspond to one standard deviation obtained from a Gaussian fit to the corresponding feature in the high-resolution scan.

Peak	eBE (cm^{-1})	eBE-EA (cm^{-1})	Assignment	KDC
A	31707(25)	-	0_0^0	-
B	32045(8)	356	4_0^1	369 (e')
C	32459(14)	770	4_0^2	777 (e')
D	32733(12)	1044	3_0^1	1069 (e')
E	32871(14)	1182	4_0^3	1152 (e')
F	33102(14)	1413	$1_0^1 4_0^1$	1424 (e')
G	33181(11)	1492	$3_0^1 4_0^1$	1494 (e')
H	33256(12)	1567	4_0^4	1579 (e')
I	33609(12)	1920	$3_0^1 4_0^2$	1931 (e')
J	33837(11)	2148	3_0^2	2157 (e')

There are several notable differences between the Weaver and cryo-SEVI spectra. First, the improvement in resolution provides a more precise EA for neutral NO_3. This is best obtained by fixing the shift from the origin for the narrowest feature in our spectrum, peak G, to the corresponding value from IR measurements, 1492 cm^{-1}, and subtracting the vibrational frequency

from this peak position in eBE. This procedure yields an EA of 3.9289(14) eV, an order of magnitude more precise than the value of 3.937(14) eV determined by Weaver *et al*. Another notable difference is the absence of the 4_1^1 feature in the cryo-SEVI spectrum. The absence of this hot band suggests negligible population of vibrationally excited anions, as is typical for cryo-SEVI experiments, where ions usually have internal temperatures on the order of 10 K.[41,43] Given the disappearance of the 4_1^1 hot band, but not the disputed 4_0^1 feature (B), in the cryo-SEVI spectrum, we can confidently reject the reassignment of the latter as the 4_1^3 hot band.[39] Peak B (**b** in Figure 2a) is indeed the originally-assigned FC-forbidden 4_0^1 transition, which gains its activity through vibronic coupling to the $\widetilde{B}^2E'$excited state, in agreement with our simulated photoelectron spectrum.

Based on the assignment of peak B, we assign C and E to the 4_0^2 and 4_0^3 transitions. The position of the 4_0^3 transition (Table 1) is consistent with previous infrared measurements in neon matrices[22] and in the gas phase.[7] In these works, the value of 1173 cm^{-1} for the *e'* sublevel of $3\nu_4$ has been confirmed by both isotopic and rotational analyses, respectively, leaving no dispute about this assignment to the $l = \pm 1$ vibrational angular momentum sublevels of the NO_3 $\nu_4 = 3$ state.

FC-forbidden features such as B acquire non-zero intensity through pJT-coupling to an excited electronic state with appropriate symmetry.[44] Within the (crude) Born-Oppenheimer approximation, the $\nu_4 = 1$ level of the $\widetilde{X}^2A'_2$ state and $\nu_4 = 0$ level of the $\widetilde{B}^2E'$ state can be written as $|a_0\rangle = |v_4 = 1\rangle|^2A_2'\rangle$ and $|b_0\rangle = |v_4 = 0\rangle|^2E'\rangle$, respectively; the transition from the anion ground state $|0\rangle = |v = 0\rangle|^1A_1'\rangle$ to $|a_0\rangle$ is FC-forbidden because the ν_4 mode is not totally symmetric,

whereas photodetachment to $|b_0\rangle$ is FC-allowed. However, states $|a_0\rangle$ and $|b_0\rangle$ each have overall *E'* vibronic symmetry and can thus mix by pJT-coupling, leading to two new states $|a\rangle = c_{1a}|a_0\rangle + c_{1b}|b_0\rangle$ and $|b\rangle = c_{2a}|a_0\rangle + c_{2b}|b_0\rangle$, each of which is an admixture of the two zero-order vibronic levels. By this vibronic coupling mechanism, the 4_0^1 transition acquires intensity and can be observed. A similar mechanism applies to the 4_0^3 transition (E).

The role of vibronic coupling can also be seen in the dependence of peak intensities and photoelectron angular distributions on the eKE. The spectra in Figure 2 show that the relative intensity of the vibrational origin (A) is much higher in the Weaver spectrum than in any of the cryo-SEVI spectra, a consequence of the lower photon energies used in the current work. This intensity dependence is explored in greater detail in Figure 3a, in which three cryo-SEVI spectra taken at different photon energies and normalized to the intensity of peak B are shown. The integrated intensities of peaks A, B, and D (normalized to peak B) are plotted as a function of eKE for all experimental spectra in Figure 3b. These data show that at lower eKE, the intensity of peak A drops off much more than that of B and D (**a** and **b** in the Weaver spectrum). Hence, the near threshold detachment cross section of the FC-allowed peak A is very different from B, which is allowed only through pJT coupling. The similar intensity dependence of B and D suggests that vibronic coupling is also responsible for a substantial portion of the intensity of D, as discussed in more detail below.

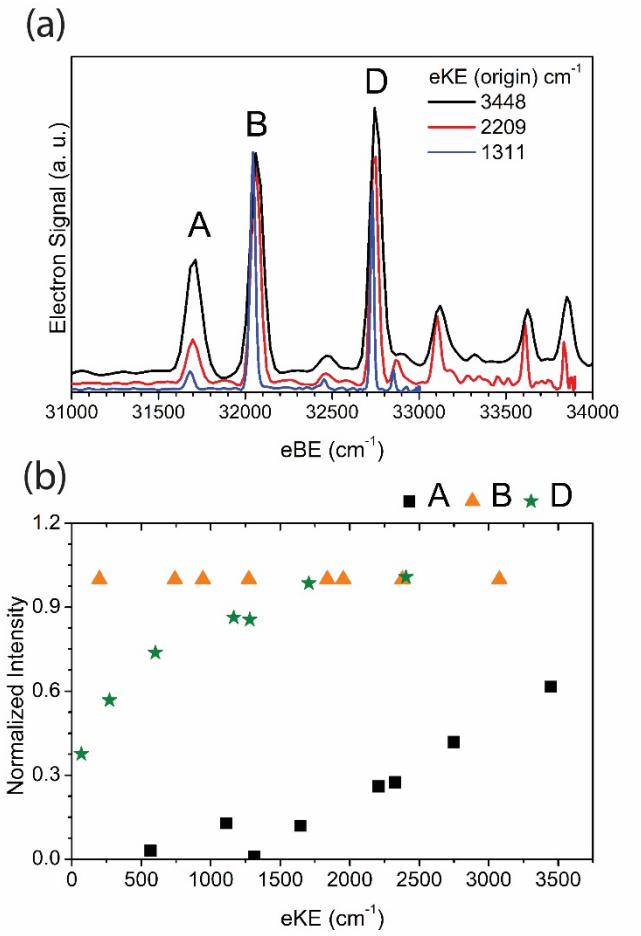

Figure 3. (a) Cryo-SEVI spectra of NO_3^- at several photon energies illustrating the differing signal attenuation for features A, B, and D as eKE decreases. The intensity of each scan has been normalized to the 4_0^1 feature. Photon energies used are 35137 (black), 33898 (red), and 32801 cm^{-1} (blue). (b) Integrated intensities of features A, B, and D, normalized to B in each scan, for all cryo-SEVI data.

The PADs were also determined at multiple photon energies. The functional form of a PAD is given by[45]

$$\frac{d\sigma}{d\Omega} = \frac{\sigma_{tot}}{4\pi}[1 + \beta P_2(\cos\theta)], \qquad (1)$$

where σ_{tot} is the total detachment cross section, $P_2(x)$ is the second-order Legendre polynomial, θ is the angle of the outgoing photoelectron with respect to the laser polarization axis, and β is the anisotropy parameter, which ranges from -1 (perpendicular detachment) to +2 (parallel detachment). Figure 4 shows β for peaks A, B, and D as a function of photon energy. Clearly, not only the intensity but also the PAD of A exhibits a markedly different energy dependence that those of B and D.

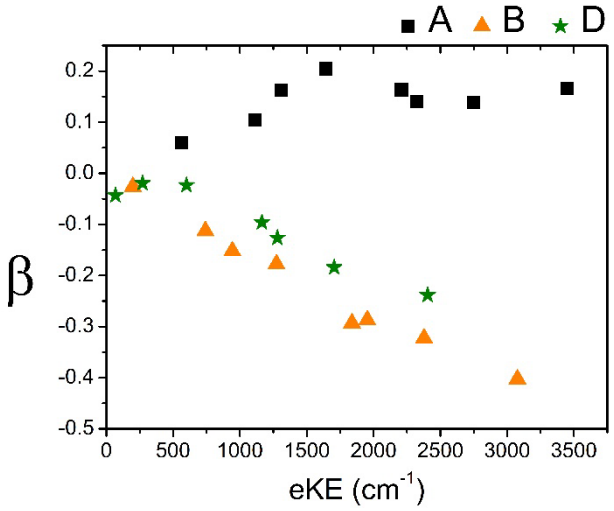

Figure 4. Measured anisotropy parameter, β, of the features A, B, and D extracted from spectra obtained at multiple photon energies.

The pJT-coupling mechanism is reflected in the striking differences in the eKE-dependent intensities and PADs of A and B. We first consider Figure 3, which shows that as the eKE is lowered, the intensity of the FC-allowed peak (A) is suppressed relative to the vibronically-allowed peak (B). This effect arises because photodetachment cross sections at low eKE are governed by the Wigner threshold law,[46]

$$\sigma \propto (\text{eKE})^{l+1/2}, \qquad (2)$$

where σ is the detachment cross section and l is the angular momentum of the detached electron. Thus, at low eKEs, the lowest-l detachment channels dominate. For detachment to the $\widetilde{X}^2A'_2$ state of NO_3, selection rules for molecular photodetachment prohibit detachment of $l = 0$ electrons, and p-wave detachment dominates. Hence, the cross section for a FC-allowed transition to the $\widetilde{X}^2A'_2$ state, such as the 0_0^0 transition, drops precipitously as the eKE is lowered.

In contrast, the 4_0^1 transition terminates in a neutral level with some contribution from the $\tilde{B}^2E'$ electronic state, detachment to which can proceed via $l = 0$ (s-wave) detachment. The less severe near-threshold attenuation of s-wave detachment then yields the observed enhancement in relative intensity of the 4_0^1 vs. the 0_0^0 transition as eKE is lowered. This situation, in which FC-allowed transitions are suppressed at low eKE relative to pJT-active features, was seen in the cryo-SEVI spectrum of the indenyl anion,[47] though the effect is much more pronounced here because the total cross section for detachment to the $\widetilde{X}^2A'_2$ state is relatively low, as discussed previously.[25] Hence, a small amount of vibronic mixing with the $\tilde{B}^2E'$ state markedly affects the intensity of a pJT-active transition.

These effects also govern the eKE-dependent PADs in Figure 4. Differing PADs in a single photodetachment band are a clear signature of vibronic coupling effects.[48,49] As the PAD reflects the angular momentum of the detached electron,[50] the partial wave components that play a role in Eq. (2) are intimately connected to the PADs of different detachment transitions, and differences in threshold behavior tend to occur together with different PADs.[49,51] This is true in NO_3, where the PAD for A is consistent with p-wave detachment, while B displays the expected trend for a

transition comprising of *s*- and *d*-wave detachment. The disparity in the PADs of A and B, coupled with their threshold behavior, unequivocally shows that B gains its intensity through pJT-coupling.

We now consider peak D. Its relative intensity remains high even at eKEs below 100 cm^{-1}, and its anisotropy parameter β becomes increasingly negative as the photon energy increases, showing similar behavior to peak B. These two trends suggest that D gains much of its intensity through the same pJT-coupling mechanism as B, and is not solely the FC-allowed 1_0^1 transition assigned previously. Only two states of *e*' symmetry, the appropriate symmetry to pJT-couple to the $\widetilde{B}^2E'$ state, plausibly reside near this feature, namely $3\nu_4$ and the ν_3 fundamental. As E has been assigned to the 4_0^3 transition both here and via IR spectroscopy, D is then dominated by the 3_0^1 transition.[27]

The identification of the pJT-coupled 3_0^1 transition in our spectrum provides the first published experimental evidence confirming the theoretical prediction that ν_3 lies well below 1492 cm^{-1}, and the predicted frequency (1069 cm^{-1})[26] is in reasonable agreement with our experimental value of 1044(16) cm^{-1}. The 1_0^1 transition cannot be observed directly as it attenuates too rapidly near threshold, where cryo-SEVI could otherwise achieve sufficient resolution[47] to observe the splitting between the ν_1 and ν_3 fundamentals.

Our findings address recently posed questions regarding the photoelectron spectrum of NO_3^-, refute the reassignment of B as the 4_1^3 hot band, and provide the first experimental confirmation that the ν_3 fundamental resides several hundred cm^{-1} below the 1492 cm^{-1} band to which it has been assigned and within 10 cm^{-1} of the ν_1 fundamental. Together, these results inform an understanding of vibronic coupling in the $\widetilde{X}^2A'_2$ ground state of NO_3 that should lessen the

controversy surrounding both the vibrational level structure of this radical and the extent that vibronic coupling manifests in the ground electronic state.

ACKNOWLEDGMENTS

The research conducted at UC Berkeley is funded by the Air Force Office of Scientific Research under Grant No. FA9550-19-1-0051 and the work done at Florida is supported by the Department of Energy, Office of Science, Office of Basic Energy Sciences under Award DE-FG02-07ER15884. M.C.B. thanks the Army Research Office for a National Defense Science and Engineering Graduate fellowship.

ASSOCIATED CONTENT

Supporting Information Available: Experimental methods, theoretical methods, Tables S1 and S2.

REFERENCES

(1) Chappuis, J. Étude spectroscopique sur l'ozone *Ann. L'Ecole Norm. Sup.* **1882**, *11*, 137.
(2) Monks, P. S. Gas-phase radical chemistry in the troposphere *Chem Soc Rev* **2005**, *34*, 376.
(3) Brown, S. S.; Stutz, J. Nighttime radical observations and chemistry *Chem Soc Rev* **2012**, *41*, 6405.
(4) Macintyre, H. L.; Evans, M. J. Sensitivity of a global model to the uptake of N_2O_5 by tropospheric aerosol *Atmos Chem Phys* **2010**, *10*, 7409.
(5) Tie, X.; Brasseur, G.; Emmons, L.; Horowitz, L.; Kinnison, D. Effects of aerosols on tropospheric oxidants: A global model study *J Geophys Res-Atmos* **2001**, *106*, 22931.
(6) Kawaguchi, K.; Fujimori, R.; Tang, J.; Ishiwata, T. Infrared spectroscopy of the NO_3 radical from 2000 to 3000 cm^{-1} *J. Mol. Spectrosc.* **2018**, *344*, 6.
(7) Kawaguchi, K.; Fujimori, R.; Ishiwata, T. Infrared spectroscopy of the $\nu_1 + \nu_4$ and $3\nu_4$ bands of the nitrate radical *J. Mol. Spectrosc.* **2018**, *347*, 56.
(8) Kawaguchi, K.; Narahara, T.; Fujimori, R.; Tang, J.; Ishiwata, T. Infrared spectroscopy of $2\nu_4$ and $\nu_3+2\nu_4$ bands of the NO_3 radical *J. Mol. Spectrosc.* **2017**, *334*, 10.
(9) Kawaguchi, K.; Fujimori, R.; Tang, J.; Ishiwata, T. On the vibrational assignment in the ground electronic state of NO_3 *J. Mol. Spectrosc.* **2015**, *314*, 73.
(10) Kawaguchi, K.; Fujimori, R.; Tang, J.; Ishiwata, T. FTIR Spectroscopy of NO_3: Perturbation Analysis of the $\nu_3+\nu_4$ State *J. Phys. Chem. A* **2013**, *117*, 13732.

(11) Fujimori, R.; Shimizu, N.; Tang, J.; Ishiwata, T.; Kawaguchi, K. Fourier transform infrared spectroscopy of the v_2 and $v_4$bands of NO_3 *J. Mol. Spectrosc.* **2013**, *283*, 10.
(12) Kawaguchi, K.; Shimizu, N.; Fujimori, R.; Tang, J.; Ishiwata, T.; Tanaka, I. Fourier transform infrared spectroscopy of the v_3 hot band of NO3 *J. Mol. Spectrosc.* **2011**, *268*, 85.
(13) Kawaguchi, K.; Ishiwata, T.; Hirota, E.; Tanaka, I. Infrared spectroscopy of the NO_3 radical *Chem. Phys.* **1998**, *231*, 193.
(14) Ishiwata, T.; Tanaka, I.; Kawaguchi, K.; Hirota, E. High-Resolution Infrared-Spectroscopy of NO_3 in the 2500 cm^{-1} Region *J. Mol. Spectrosc.* **1992**, *153*, 167.
(15) Kawaguchi, K.; Ishiwata, T.; Tanaka, I.; Hirota, E. Fourier-Transform Infrared-Spectroscopy of the NO_3 Radical *Chem. Phys. Lett.* **1991**, *180*, 436.
(16) Nelson, H. H.; Pasternack, L.; Mcdonald, J. R. Laser-induced excitation and emission spectra of nitrate radical (NO_3) *Journal of Physical Chemistry* **1983**, *87*, 876.
(17) Ishiwata, T.; Fujiwara, I.; Naruge, Y.; Obi, K.; Tanaka, I. Study of NO_3 by Laser-Induced Fluorescence *Journal of Physical Chemistry* **1983**, *87*, 1349.
(18) Kim, B. S.; Hunter, P. L.; Johnston, H. S. NO_3 Radical Studied by Laser-Induced Fluorescence *J. Chem. Phys.* **1992**, *96*, 4057.
(19) Hirota, E.; Ishiwata, T.; Kawaguchi, K.; Fujitake, M.; Ohashi, N.; Tanaka, I. Near-infrared band of the nitrate radical NO_3 observed by diode laser spectroscopy *J. Chem. Phys.* **1997**, *107*, 2829.
(20) Ishiwata, T.; Tanaka, I. K., K. ; Hirota, E. Infrared diode laser spectroscopy of the NO_3 v_3 band *J. Chem. Phys.* **1985**, *82*, 2196.
(21) Jacox, M. E.; Thompson, W. E. A^2E''-X^2A_2' Transition of NO_3 Trapped in Solid Neon *J. Phys. Chem. A* **2010**, *114*, 4712.
(22) Jacox, M. E.; Thompson, W. E. The infrared spectroscopy and photochemistry of NO_3 trapped in solid neon *J. Chem. Phys.* **2008**, *129*.
(23) Codd, T.; Chen, M. W.; Roudjane, M.; Stanton, J. F.; Miller, T. A. Jet cooled cavity ringdown spectroscopy of the A^2E'' <- X^2A_2' transition of the NO_3 radical *J. Chem. Phys.* **2015**, *142*.
(24) Okumura, M.; Stanton, J. F.; Deev, A.; Sommar, J. New insights into the Jahn-Teller effect in NO_3 via the dark A^2E'' state *Phys. Scr.* **2006**, *73*, C64.
(25) Weaver, A.; Arnold, D. W.; Bradforth, S. E.; Neumark, D. M. Examination of the $^2A_2'$ and $^2E''$ States of NO_3 by ultraviolet photoelectron spectroscopy of NO_3^- *J. Chem. Phys.* **1991**, *94*, 1740.
(26) Simmons, C. S.; Ichino, T.; Stanton, J. F. The v_3 Fundamental in NO_3 Has Been Seen Near 1060 cm^{-1}, Albeit Some Time Ago *J. Phys. Chem. Lett.* **2012**, *3*, 1946.
(27) Stanton, J. F. On the vibronic level structure in the NO_3 radical. I. The ground electronic state *J. Chem. Phys.* **2007**, *126*.
(28) Mukherjee, B.; Mukherjee, S.; Sardar, S.; Shamasundar, K. R.; Adhikari, S. A beyond Born-Oppenheimer treatment of five state molecular system NO_3 and the photodetachment spectra of its anion *Chem. Phys.* **2018**, *515*, 350.
(29) Mayer, M.; Cederbaum, L. S.; Koppel, H. Ground-State Dynamics of NO_3 - Multimode Vibronic Borrowing Including Thermal Effects *J. Chem. Phys.* **1994**, *100*, 899.
(30) Faraji, S.; Koppel, H.; Eisfeld, W.; Mahapatra, S. Towards a higher-order description of Jahn-Teller coupling effects in molecular spectroscopy: The A_2E'' state of NO_3 *Chem. Phys.* **2008**, *347*, 110.

(31) Eisfeld, W.; Morokuma, K. *Ab initio* investigation of the vertical and adiabatic excitation spectrum of NO_3 *J. Chem. Phys.* **2001**, *114*, 9430.
(32) Davy, R. D.; Schaefer, H. F. Is There an Absence of Threefold Symmetry at the Equilibrium Geometry of the Ground Electronic State for NO_3 *J. Chem. Phys.* **1989**, *91*, 4410.
(33) Kaldor, U. The Ground-State Geometry of the NO_3 Radical *Chem. Phys. Lett.* **1990**, *166*, 599.
(34) Stanton, J. F.; Gauss, J.; Bartlett, R. J. On the Choice of Orbitals for Symmetry-Breaking Problems with Application to NO_3 *J. Chem. Phys.* **1992**, *97*, 5554.
(35) Stanton, J. F.; Gauss, J.; Bartlett, R. J. Potential Nonrigidity of the NO_3 Radical *J. Chem. Phys.* **1991**, *94*, 4084.
(36) Kim, B.; Hammond, B. L.; Lester, W. A.; Johnston, H. S. *Ab initio* Study of the Vibrational-Spectra of NO_3 *Chem. Phys. Lett.* **1990**, *168*, 131.
(37) Beckers, H.; Willner, H.; Jacox, M. E. Conflicting Observations Resolved by a Far IR and UV/Vis Study of the NO_3 Radical *Chem. Phys. Chem.* **2009**, *10*, 706.
(38) Ishiwata, T.; Nakano, Y.; Kawaguchi, K.; Hirota, E.; Tanaka, I. Analyses of the Infrared Absorption Bands of $^{15}NO_3$ in the 1850-3150 cm^{-1} Region *J. Phys. Chem. A* **2010**, *114*, 980.
(39) Hirota, E. Assignment of the photoelectron spectrum of the nitrate anion NO_3^- and vibronic interactions in the nitrate free radical *J. Mol. Spectrosc.* **2018**, *343*, 81.
(40) Yamada, K.; Ross, S.96th Ann. Meeting Chem. Soc. Jpn. Kyotanabe, Kyoto, Japan 2016, Paper 2E6-28
(41) Hock, C.; Kim, J. B.; Weichman, M. L.; Yacovitch, T. I.; Neumark, D. M. Slow photoelectron velocity-map imaging spectroscopy of cold negative ions *J. Chem. Phys.* **2012**, *137*.
(42) Koppel, H.; Domcke, W.; Cederbaum, L. S. Multimode Molecular-Dynamics Beyond the Born-Oppenheimer Approximation *Adv Chem Phys* **1984**, *57*, 59.
(43) Kim, J. B.; Hock, C.; Yacovitch, T. I.; Neumark, D. M. Slow Photoelectron Velocity-Map Imaging Spectroscopy of Cold Thiozonide (S_3^-) *J. Phys. Chem. A* **2013**, *117*, 8126.
(44) Herzberg, G. *Electronic Spectra and Electronic Structure of Polyatomic Molecules*; Van Nostrand Reinhold Company: Princeton, NJ, 1966; Vol. 3.
(45) Cooper, J.; Zare, R. N. Angular Distribution of Photoelectrons *J. Chem. Phys.* **1968**, *48*, 942.
(46) Wigner, E. P. On the Behavior of Cross Sections near Thresholds *Phys. Rev.* **1948**, *73*, 1002.
(47) Kim, J. B.; Weichman, M. L.; Yacovitch, T. I.; Shih, C.; Neumark, D. M. Slow photoelectron velocity-map imaging spectroscopy of the C_9H_7 (indenyl) and $C_{13}H_9$ (fluorenyl) anions *J. Chem. Phys.* **2013**, *139*.
(48) Ervin, K. M.; Lineberger, W. C. Photoelectron-Spectra of C_2^- and C_2H- *Journal of Physical Chemistry* **1991**, *95*, 1167.
(49) DeVine, J. A.; Taka, A. A.; Babin, M. C.; Weichman, M. L.; Hratchian, H. P.; Neumark, D. M. High-resolution photoelectron spectroscopy of TiO3H2-: Probing the TiO2- + H2O dissociative adduct *J. Chem. Phys.* **2018**, *148*, 222810.
(50) Sanov, A. Laboratory-Frame Photoelectron Angular Distributions in Anion Photodetachment: Insight into Electronic Structure and Intermolecular Interactions *Annu. Rev. Phys. Chem.* **2014**, *65*, 341.

(51) Babin, M. C.; DeVine, J. A.; Weichman, M. L.; Neumark, D. M. Slow photoelectron velocity-map imaging of cold C_7^- and C_9^- *J. Chem. Phys.* **2018**, *149*.